Chemical Engineering Journal 387 (2020) 124165

Contents lists available at ScienceDirect

Chemical Engineering Journal

journal homepage: www.elsevier.com/locate/cej

Activation of peroxydisulfate by natural titanomagnetite for atrazine removal via free radicals and high-valent iron-oxo species

Leiduo Lai[a,b], Hongyu Zhou[a,b], Heng Zhang[a,b], Zhimin Ao[c], Zhicheng Pan[d], Qixuan Chen[e], Zhaokun Xiong[a,b,*], Gang Yao[b,f], Bo Lai[a,b,*]

[a] State Key Laboratory of Hydraulics and Mountain River Engineering, College of Architecture and Environment, Sichuan University, Chengdu 610065, China
[b] Sino-German Centre for Water and Health Research, Sichuan University, Chengdu 610065, China
[c] Guangdong Key Laboratory of Environmental Catalysis and Health Risk Control, Institute of Environmental Health and Pollution Control, School of Environmental Science and Engineering, Guangdong University of Technology, Guangzhou 51006, China
[d] Laboratory of Wastewater Treatment Technology in Sichuan Province, Haitian Water Group, China
[e] Department of Chemical Engineering, Imperial College London, South Kensington Campus, London SW7 2AZ, UK
[f] Institute of Environmental Engineering, RWTH Aachen University, Germany

HIGHLIGHTS

- The natural titanomagnetite was used for the first time as a PDS activator to remove ATZ.
- Both free radicals and high-valent iron-oxo species were found in heterogeneous titanomagnetite/PDS system.
- The reaction mechanism of reactive oxygen species in titanomagnetite/PDS system were studied in depth.
- ATZ degradation pathways in titanomagnetite/PDS system were proposed.

GRAPHICAL ABSTRACT

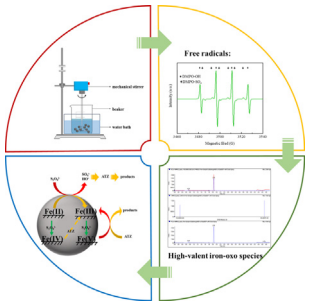

ARTICLE INFO

Keywords:
Atrazine
Titanomagnetite
High-valent iron-oxo species
Reaction mechanism

ABSTRACT

Natural titanomagnetite, a potential catalyst, was used as a peroxydisulfate (PDS) activator for the removal of atrazine (ATZ) in water for the first time. The surface ≡Fe(II) and ≡Fe(III) of titanomagnetite was certified as the active components by XRD and XPS analyses. ATZ removal showed a strong dependence on the titanomagnetite concentration (0–10 g/L), PDS concentration (0–10 mM) and the initial pH (3.0–11.0) under experimental conditions. Quite different from the traditional heterogeneous PDS-activated processes, titanomagnetite/PDS system could remove ATZ via both radical and nonradical pathways. Here, both free radicals ($SO_4^{\cdot -}$ and $HO^{\cdot}$) and high-valent iron-oxo species were proved to be the main reactive oxygen species (ROS) by quenching experiments, EPR tests and UPLC/ESI–MS/MS analysis. The high-valent iron-oxo species, ≡Fe^{IV}=O and ≡Fe^{V}=O, could be generated from the ≡Fe(II) and ≡Fe(III) of the titanomagnetite via a nonradical pathway. In addition, the generated passivation layer after reaction was found via XPS analysis, which could block the function of ≡Fe(II) and ≡Fe(III), hindering the generation of ROS. However, the catalytic activity of titanomagnetite could recover if passivation layer was removed by ultrasonic cleaning. Finally, ten intermediates of ATZ were measured by UPLC-QTOF-MS/MS and the degradation pathways of ATZ in titanomagnetite/PDS system were proposed with the Gaussian 09 results. This work helps to better understand the generation of high-

* Corresponding authors at: State Key Laboratory of Hydraulics and Mountain River Engineering, College of Architecture and Environment, Sichuan University, Chengdu 610065, China.
E-mail addresses: scuxzk@scu.edu.cn (Z. Xiong), laibo@scu.edu.cn (B. Lai).

https://doi.org/10.1016/j.cej.2020.124165
Received 9 October 2019; Received in revised form 15 January 2020; Accepted 18 January 2020
Available online 21 January 2020

valent iron-oxo species and re-evaluate the effect of high-valent iron-oxo species in the heterogeneous iron-based PDS-activated processes.

1. Introduction

Atrazine (ATZ) is a low-cost and highly effective herbicide [1,2], which has been widely used in various countries due to agricultural development [3]. In China, ATZ was initially introduced in the early 1980s and its usage had increased rapidly in the late 1990s. Due to overuse, ATZ has been extensively detected in related aquatic environment [4,5], which has been caught attention in public and academic community.

According to previous studies, ATZ could not only affect the growth and reproduction of aquatic organisms but also increase the risk of getting cancer for human beings [6,7]. To ensure human health and protect environment, various countries have regulated the relevant standards to limit the concentration of ATZ in waters [8,9]. However, traditional biological treatment technology can hardly meet these standards due to the degradation-resistant nature of ATZ. Therefore, it is urgent to develop an efficient way to degrade ATZ.

Sulfate radical ($SO_4^{\cdot -}$) based advanced oxidation processes (AOPs) have been extensively investigated because of their outstanding advantages in degrading new pollutants, such as perfluorocarboxylic acids, pesticides, pharmaceutical and personal care products (PPCPs) [10–14]. $SO_4^{\cdot -}$ is mainly derived from the electron transfer of peroxydisulfate (PDS, $S_2O_8^{2-}$) and peroxymonosulfate (PMS, HSO_5^-) [15–17]. Compared with PMS, PDS cannot spontaneously decompose to generate reactive oxygen species (ROS) due to its symmetrical structure. In recent studies, many researchers are keen on activating PDS by using various types of solid catalysts, including carbon-based materials [18–20], synthetic metals catalysts [21–23], nano materials [24] and chelated or unchelated transition metal-based catalysts [25,26], *etc.* Usually, iron-based materials are considered as the most satisfying catalysts since they are environmentally friendly and cost-effective [27]. Table S1 summarizes relevant studies about PDS or PMS activation by different iron-based catalysts. It is widely accepted that iron-based catalysts could activate PDS to form $SO_4^{\cdot -}$ and hydroxyl radical ($HO^{\cdot}$) simultaneously due to reaction of $SO_4^{\cdot -}$ with H_2O and HO^-. Recently, some researchers have found that instead of free radicals, high-valent iron-oxo species of $\equiv Fe^{IV}=O$ were generated in homogeneous Fe(II)/PDS and Fe(II)/PMS systems [28,29]. In addition, high-valent iron-oxo species of $\equiv Fe^{V}=O$ were also detected when Fe(III) doped gC_3N_4 was used as a heterogeneous PMS activator [30]. In general, those iron-based catalysts were either Fe^{2+} in liquid or synthetic. However, to the best of our knowledge, it is not clear so far whether high-valent iron-oxo species can be formed when natural heterogeneous iron-based catalysts are used to activate PDS.

Titanomagnetite, a composite natural mineral, is also an iron-based material, of which $(Fe_{2.5}Ti_{0.5})_{1.04}O_4$, $FeTiO_3$ and Fe_3O_4 are primary components. Titanomagnetite is usually used as the material for melting of iron and titanium, but its performance in PDS activation systems has never been investigated. Hence, we used titanomagnetite as a PDS activator to establish a titanomagnetite/PDS system to evaluate its performance in ATZ removal and investigate the generation mechanism of ROS. The objectives of this study are to (1) investigate the effects of key operational parameters on ATZ removal; (2) detect the main ROS and explore the generation mechanism of high-valent iron-oxo species ($\equiv Fe^{IV}=O$ and $\equiv Fe^{V}=O$); (3) verify the formation of passivation layer and explore the impact of adsorbates in the catalyst deactivation; (4) analyze the degradation pathways of ATZ.

2. Materials and methods

2.1. Reagents

Sources of chemicals are provided in the Supporting Information (SI) Text S1.

2.2. Experiment procedure

In this study, the stock solution of ATZ was prepared in advance. At each run, 150 mL of ATZ stock solution (10 mg/L) and known amounts of titanomagnetite (3–10 g/L) and PDS (2–10 mM) were simultaneously added to a 250 mL beaker to initiate the reaction. The initial pH of ATZ stock solution without adjusting was 6.3. Furthermore, 1 mM NaOH and H_2SO_4 were used to adjust the initial pH (3.0–11.0). To ensure complete contact of catalysts, oxidants and contaminants, the reaction was equipped with a mechanical stir bar at 300 rpm. As well, the reaction temperature was controlled at 30 ± 1 °C by a water bath. The whole reaction time was 90 min. To detect the degradation of ATZ during the reaction process, 2 mL of sample was collected from the solution at predetermined times and filtered through 0.45 μm PTFE syringe filter discs. At the same time, excess (500 mM) EtOH and TBA used as scavengers were added to the sample to quench the free radicals. All data shown in this study were obtained after repeating three times. Meanwhile, the error bars in the figures stand for standard deviation of the means.

2.3. Analytical method

The concentration of ATZ during the reaction process was quantified by a reversed-phase high performance liquid chromatography system (HPLC, Agilent USA) equipped with the Eclipse XDB C-18 (5 μm, 4.6 × 250 mm) column. The mobile phase was mixed with ultrapure water (20%) and methanol (80%). As well, the flow rate of the mobile phase was set at 1.0 mL/min and the test wavelength was set at λ = 225 nm. The total organic carbon (TOC) removal was analyzed via a TOC analyzer (Shimazu, Japan). The PDS consumptions in reaction processes were measured by modificatory iodometric detection method [31]. Details about the measurement method are shown in SI Text S2. Furthermore, the dissolved Fe in the effluent was detected by inductively coupled plasma-Mass Spectrometry (ICP-MS, NexION, 300X, PerkinElmer, USA). The NO_3^- in the effluent was detected by ion chromatography system (Thermofisher, ICS-600). The phase analysis of titanomagnetite was studied by X-ray powder diffraction (XRD, PANalytical B.V., Holland). Elementary compositions of titanomagnetite were detected by an energy dispersive spectrometer and (EDS, SU8010, Hitachi, Japan). The nitrogen gas uptake isotherms were analyzed by Micromeritics ASAP 2460 (Micromeritics, USA) and the specific surface areas (SSAs) were calculated based on Brunauer-Emmett-Teller (BET) model. The chemical states of Fe, O, Ti and S were detected by an X-ray photoelectron spectroscopy (XPS, AXIS Ultra DLD, Kratos Co., UK). Free radicals generated in this system were detected by electron paramagnetic resonance (EPR, Bruker, Germany). High-valent iron-oxo species were indirectly studied by UPLC/ESI-MS/MS systems. The degradation intermediates of ATZ were analyzed via ultrahigh performance liquid chromatograph (Agilent, 1290 Infinity II) coupled with an AgilentG6545 Q-TOF mass spectrometry (UPLC-QTOF-MS/MS). The details are provided in the SI Text S3.

3. Results and discussion

3.1. Characteristics of titanomagnetite

It is well illustrated from the XRD pattern (Fig. 1(a)) that the compositions of the natural titanomagnetite are titanomagnetite ($(Fe_{2.5}Ti_{0.5})_{1.04}O_4$), ilmenite ($FeTiO_3$) and magnetite ($Fe_3O_4$), indicating Ti and Fe were the principal elements in the titanomagnetite. To quantify the percentage of these three minerals in titanomagnetite, EDS was used in this study. EDS-mappings were tested three times to take the mean to eradicate any discrepancies (Fig. S1). There were 56.29% Fe, 15.32% Ti and 28.39% O in the natural titanomagnetite. According to the stoichiometric ratio, it could be calculated that the proportions of titanomagnetite, ilmenite and magnetite were 70%, 25% and 5%, respectively. In general, instead of Ti, Fe was the active species for PDS activation. Therefore, the main active element, Fe, in the titanomagnetite was analyzed by XPS experiments (Fig. 1(b)). There were two peaks located at 711.5 eV and 712.3 eV for Fe 2p3/2, representing the Fe(II) and Fe(III) on the surface sites of titanomagnetite, respectively. In other words, both ≡Fe(II) and ≡Fe(III) existed in the titanomagnetite, which might facilitate the PDS activation for ATZ removal. Furthermore, the magnetism of titanomagnetite is shown in Fig. S2, suggesting titanomagnetite is easily recycled and restraining the secondary pollution.

3.2. Degradation of ATZ in different systems

The efficiency of ATZ removal was investigated in three systems (i.e., titanomagnetite/PDS, PDS alone and titanomagnetite alone systems). Fig. 2 (a) shows neither titanomagnetite (1%) nor PDS alone (5%) had effects on ATZ removal, which might be the absence of the generation of ROS. Excellent removal efficiency of ATZ (92%) could be only achieved in titanomagnetite/PDS system, implying the efficient activation effect of titanomagnetite on PDS. Moreover, ATZ removal during the treatment process was fitted by the pseudo-first-order kinetic model. The kinetic rate constant can be calculated as Eq. (1):

$$-\frac{d[ATZ]}{dt}=k_{obs}[ATZ] \quad (1)$$

where k_{obs} represents the pseudo-first-order rate constants (min^{-1}), t stands for the reaction time (min) and [ATZ] represent the concentration of ATZ. Fig. 2(b) suggests the k_{obs} in titanomagnetite/PDS system (2.5×10^{-2} min^{-1}) was 79.4 times and 416.7 times of that in the PDS alone (3.15×10^{-4} min^{-1}) and titanomagnetite alone (0.6×10^{-4} min^{-1}) systems. Here, enhancement ratio (f) [32,33] (Eq. (2)) was introduced to quantify the enhancement of titanomagnetite/PDS system for ATZ removal. If $f > 1$, indicating there was an enhancement effect on ATZ removal in titanomagnetite/PDS system. If f less than 1, indicating an inhibition effect on ATZ removal. Besides, if $f = 1$, the removal efficiency of ATZ in the titanomagnetite/PDS system was simply the sum of ATZ removal in PDS alone and titanomagnetite alone systems. According to Eq. (2), the calculated f was 66.7, suggesting an excellent catalytic effect of titanomagnetite on PDS activation.

$$f=\frac{k_{obs\ titanomagnetite/PS}}{k_{obs\ PS\ alone\ system}+k_{obs\ titanomagnetite\ alone\ system}} \quad (2)$$

Fig. 2(c) shows that TOC removal (about 32%) in titanomagnetite/PDS system was much more than that (1% and 1%, respectively) in PDS and titanomagnetite alone systems. The results convincingly demonstrated that the satisfactory removal efficiency of ATZ in titanomagnetite/PDS system thanks to the effective catalytic performance of titanomagnetite to PDS. Furthermore, to better illustrate the mechanism of PDS activation by titanomagnetite, PDS consumptions in reaction processes in titanomagnetite/PDS and PDS alone systems were detected. Fig. 2(d) suggested PDS was hardly decomposed into ROS without titanomagnetite. Thus, ATZ removal efficiency was limited in PDS alone system. However, once titanomagnetite added, PDS could be decomposed effectively, leading to the generation of ROS and degradation of ATZ. The mechanism of ROS generation is discussed detailedly in Section 3.4.

3.3. Effect of parameters

In this section, some crucial parameters that affect ATZ removal such as titanomagnetite concentration, PDS concentration, and the initial pH, were investigated in detail.

3.3.1. Effect of titanomagnetite concentration on ATZ removal

Fig. 3(a) shows PDS without titanomagnetite can hardly degrade ATZ due to its limited oxidizability. However, the ATZ removal efficiency increased largely after adding titanomagnetite. The ATZ removal efficiency increased from 6% to 92% when titanomagnetite concentration increased from 0 to 8 g/L. Nevertheless, the final ATZ removal efficiency was not improved when titanomagnetite concentration increased from 8 to 10 g/L. To better illustrate the effect of titanomagnetite concentration on ATZ removal, PDS consumptions in treatment process were measured. Fig. S3(a) shows PDS consumptions increased with the increased concentration of titanomagnetite. The results suggested that the existence of titanomagnetite provided plentiful active sites for PDS decomposition to generate ROS. However, superfluous active sites leading to fast generation of ROS, which might

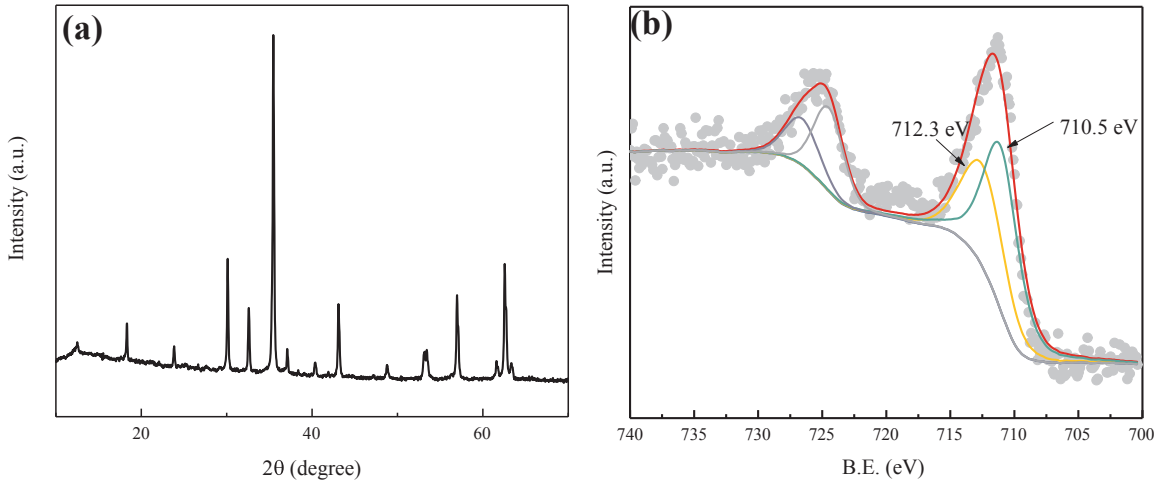

Fig. 1. XRD patterns of titanomagnetite (a) and XPS fitting result of Fe 2p in the titanomagnetite (b).

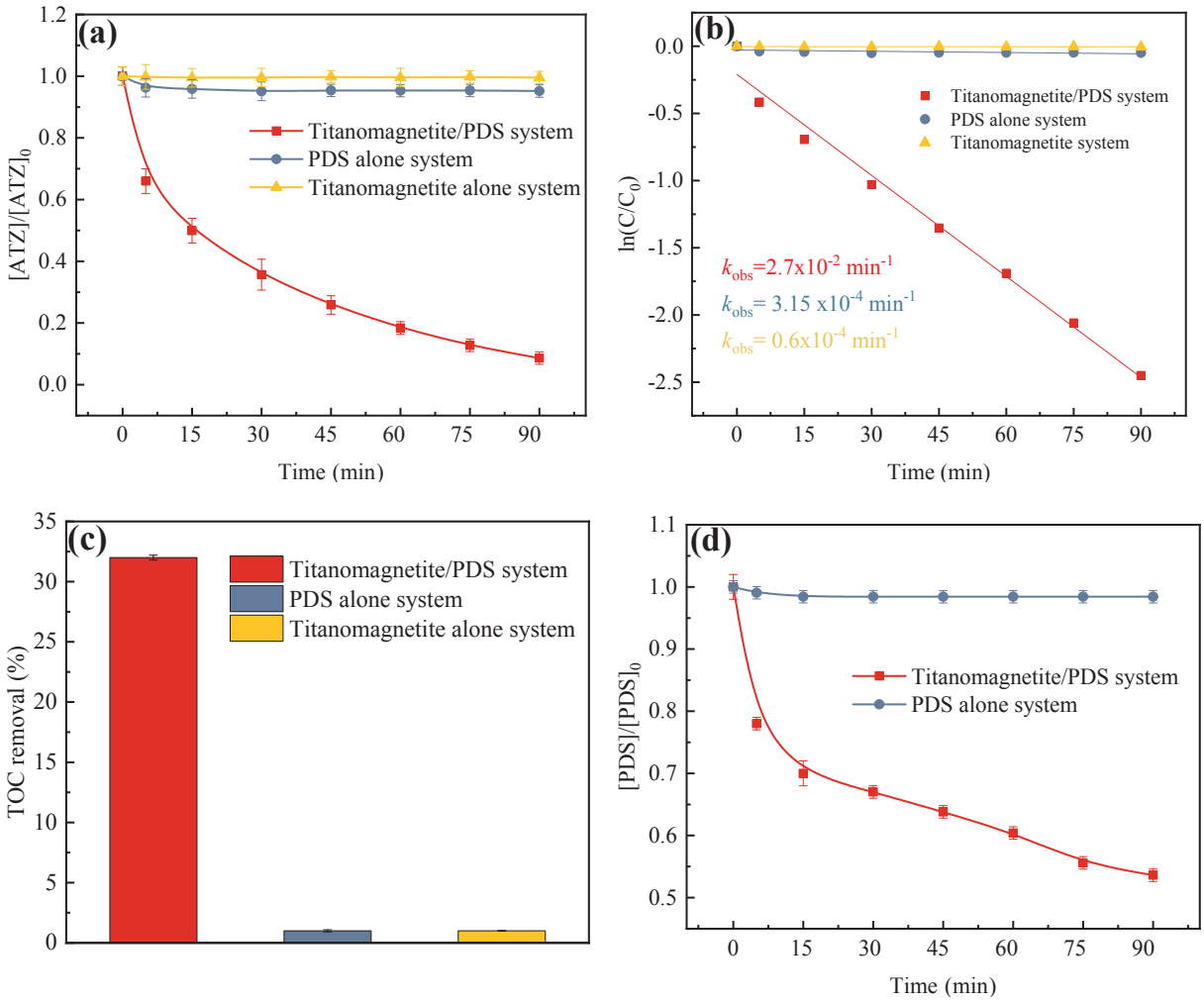

Fig. 2. The ATZ removal (a), k_{obs} (b) and TOC removal in titanomagnetite/PDS, PDS alone and titanomagnetite alone systems. PDS consumption (d) in titanomagnetite/PDS and PDS alone system. ($[ATZ]_0$ = 10 mg/L, $[PDS]_0$ = 5.0 mM, titanomagnetite = 8 g/L, initial pH = 6.3 and stirring rate = 300 rpm).

be quenched by themselves and residual PDS (Eqs. (3) and (4)). Additionally, excess titanomagnetite made the reaction between ≡Fe(II) and $SO_4^{\cdot -}$ (Eq. (5)) possible [34].

$$SO_4^{\cdot -} + SO_4^{\cdot -} S_2O_8^{2-} \quad (3)$$

$$S_2O_8^{2-} + SO_4^{\cdot -} S_2O_8^{\cdot -} + SO_4^{2-} \quad (4)$$

$$\equiv Fe(II) + SO_4^{\cdot -} \rightarrow \equiv Fe(III) + SO_4^{2-} \quad (5)$$

3.3.2. Effect of PDS concentration on ATZ removal

We can see in Fig. 3(b) that ATZ can hardly be removed without PDS. However, once PDS was added in the aqueous solution, ATZ removal efficiency raised rapidly. As the PDS concentration increased from 2 to 5 mM, the removal efficiency of ATZ rapidly increased from 69% to 92%. Nevertheless, as PDS concentration continued to increase (5–10 mM), the expected ATZ removal efficiency had never occurred. Besides, Fig. S3(b) suggests the PDS consumptions increased with the PDS concentration. The PDS consumptions signified the generation of ROS. Thus, the amount of ROS was consistent with PDS consumptions. All the results indicated that excess PDS could scavenge ROS (Eq. (4)). In addition, excessive $SO_4^{\cdot -}$ could be self-quenched due to the fast generation rate of $SO_4^{\cdot -}$ (Eq. (3)).

3.3.3. Effect of initial pH on ATZ removal

The initial pH is an important factor in pollutants removal process because it influences the pH_{zpc} of catalyst, the acid dissociation constant (p*K*a) of contaminant, and the decomposition rate of PDS, thereby affecting the removal efficiency of pollutants. In this study, the effect of initial pH on ATZ removal efficiency is shown in Fig. 3(c). Of note, the buffer chemicals like phosphate, carbonate and borate might have an adverse impact on ATZ removal efficiency. Thus, no buffer was used in this part. The ATZ removal efficiency enhanced from 80% to 100% as the initial pH decrease from 11.0 to 3.0. In other words, acidic conditions favored ATZ removal. To clarify the reason of ATZ removal trend at different initial pH, the pH changes during the treatment were examined.

It is obvious in Fig. 3(d) that the pH value during the treatment maintained around 3.0 regardless of initial pH. This could be attributed to the buffering capacity of titanomagnetite/PDS system. Once PDS and titanomagnetite were in full contact, PDS would be decomposed in large amounts and H^+ would be generated in large quantities. Therefore, a part of the PDS might not react to generate ROS, but released H^+ to carry out neutralization reaction under alkaline conditions. From this perspective, the fewer PDS involved in the reaction, the less ROS formed in reaction process. Besides, Fig. S3(c) shows the PDS consumptions at different initial pH. It was apparent that the PDS consumptions under alkaline conditions were lower than that under acidic conditions. From this perspective, the fewer PDS involved in the reaction, the less ROS formed in titanomagnetite/PDS system. Ultimately, ATZ removal efficiency was unsatisfactory under alkaline conditions.

The p*K*a of ATZ equals 1.68 [35–37], therefore, ATZ obtained a

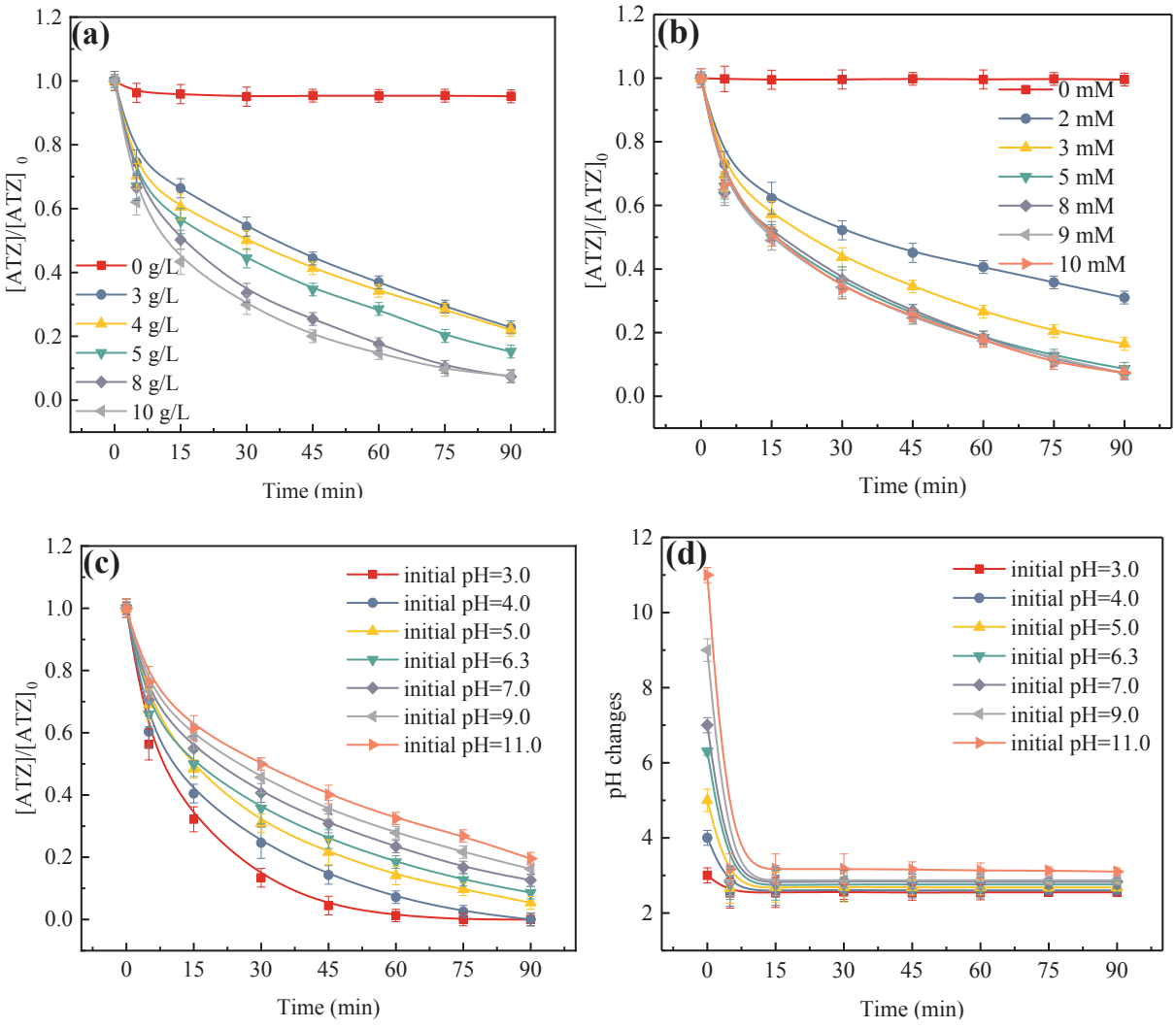

Fig. 3. Effect of titanomagnetite concentration (a), PDS concentration (b) and initial pH (c) on ATZ removal; pH value in treatment process at different initial pH (d). ($[ATZ]_0$ = 10 mg/L, $[PDS]_0$ = 5.0 mM, titanomagnetite = 8 g/L, initial pH = 6.3 and stirring rate = 300 rpm).

negative charge in the pH range of this study. Meanwhile, the pH_{zpc} of the titanomagnetite was 6.6 (seen in Fig. S4). At the initial pH < pH_{zpc}, the surface of the titanomagnetite was protonated, while the surface of titanomagnetite was deprotonated at initial pH > pH_{zpc}. Additionally, $S_2O_8^{2-}$ in the liquid is fully ionized, indicating it was in negative charges in this study. Thus, under acidic conditions, the interaction between titanomagnetite, PDS and ATZ could be enhanced. However, when the initial pH was under alkaline condition, the titanomagnetite, ATZ and $S_2O_8^{2-}$ were all negative. In other words, the electrostatic interaction between titanomagnetite, PDS and ATZ was mutually exclusive at alkaline pH, resulting in insufficient contact between titanomagnetite, PDS and ATZ. Furthermore, to exam the adsorption effect at different initial pH, BET surface area of titanomagnetite was detected and adsorption control experiments were conducted. Fig. S5(a) shows BET surface area of titanomagnetite was 3.1 m^2/g, suggesting the surface area of titanomagnetite was small. Besides, Fig. S5(b) shows the adsorption effects on ATZ removal at different initial pH. Although the ATZ removal efficiencies at acidic conditions were promoted, the adsorbed ATZ was also easy to desorption, indicating the adsorption effects could be ignored. In other words, the contact of titanomagnetite, PDS and ATZ was a physical absorption.

Besides, under alkaline conditions, a part of $SO_4^{\cdot -}$ would change into $HO^{\cdot}$, as shown in Eqs. (6) and (7). The rate constants of the reaction between $SO_4^{\cdot -}$ and ATZ ($k_{ATZ+\ SO4^{\cdot -}}$ = 3.5 ± 0.08 × 10^9 $M^{-1}s^{-1}$) is higher than that between $HO^{\cdot}$ and ATZ ($k_{ATZ+\ HO^{\cdot}}$ = (2.4–3) × 10^9 $M^{-1}s^{-1}$) [38–40]. Hence, the above three factors acted in a synergistic manner to affect the removal efficiency of ATZ.

Furthermore, by the analysis of ICP-MS, there was no dissolved iron (including Fe^{2+} and Fe^{3+}) in the effluent at different initial pH. In other words, homogeneous catalysis was not involved under acidic conditions.

$$HO^- + SO_4^{\cdot -} \rightarrow HO^{\cdot} + SO_4^{2-} \quad (6)$$

$$H_2O + SO_4^{\cdot -} \rightarrow HO^{\cdot} + SO_4^{2-} + H^+ \quad (7)$$

3.4. Detection of reactive oxygen species

3.4.1. The detection of free radicals

It was well documented that PDS/PMS-activated systems by transition metal-based materials always form free radicals like $SO_4^{\cdot -}$ and $HO^{\cdot}$ to degrade organics in the aqueous solution [41–43]. According to the capture rate of different quenchers, tert butyl alcohol (TBA) was used as an effective $HO^{\cdot}$ scavenger ($k_{TBA+\ HO^{\cdot}}$ = (3.8–7.6)X 10^8 $M^{-1}s^{-1}$, $k_{TBA\ +\ SO4^{\cdot -}}$ = (4–9.1) × 10^5 $M^{-1}s^{-1}$) [44], while ethyl alcohol (EtOH) was used as a quenching agent for both $SO_4^{\cdot -}$ and $HO^{\cdot}$ ($k_{EtOH\ +\ HO^{\cdot}}$ = 9.1 X 10^6 $M^{-1}s^{-1}$, $k_{EtOH\ +\ SO4^{\cdot -}}$ = 3.5 × 10^7 $M^{-1}s^{-1}$)

[45]. Seen in Fig. 4(a), both EtOH and TBA had quenching effects on ATZ removal efficiency, indicating generation of both $SO_4^{\cdot -}$ and $HO^{\cdot}$ in titanomagnetite/PDS system. The inhibition effect of EtOH was only slightly higher than TBA, indicating $HO^{\cdot}$ accounted for a larger proportion in the titanomagnetite/PDS system. In addition, to examine whether superoxide radical ($O_2^{\cdot -}$) existed (Eqs. (8) and (9)) [46], BQ was used as a probe (Fig. S6). The ATZ removal efficiency was slightly better than that without BQ. Thus, superoxide radical ($O_2^{\cdot -}$) was not formed in titanomagnetite/PDS system. The better removal efficiency of ATZ could be illustrated as the generation of other ROS with addition of BQ [47].

$$S_2O_8^{2-} + 2H_2O \rightarrow HO_2^- + 2SO_4^{2-} + 3H^+ \quad (8)$$

$$S_2O_8^{2-} + HO_2^- \rightarrow SO_4^{\cdot -} + SO_4^{2-} + O_2^{\cdot -} + H^+ \quad (9)$$

The EPR experiment in titanomagnetite/PDS system was conducted with DMPO, which was used as a trapping agent to analyze the dominant ROS. Fig. 4(b) shows the characteristic peaks were the signal of DMPO-OH ($a_N = a_H = 14.9$ G) and DMPO-SO_4($a_N = 13.2$ G, $a_H = 9.6$ G, $a_H = 1.48$ G and $a_H = 0.78$ G). The $HO^{\cdot}$ was detected to be the dominant ROS in the titanomagnetite/PDS system, suggesting that $SO_4^{\cdot -}$ could change into $HO^{\cdot}$ during the reaction process (Eqs. (6) and (7)) [41]. Another possibility is that the conversion of DMPO-SO_4 to DMPO-OH might occur in aqueous solution [48].

3.4.2. The detection of high-valent iron-oxo species

Recently, some researchers suggested that high-valent iron-oxo species (≡Fe^{IV}=O and ≡Fe^{V}=O), from catalyzation of PDS or PMS by Fe(II)/Fe(III), could also make a contribution for contaminants degradation [28,30]. Thus, the presence of high-valent iron-oxo species should be studied in this study.

It is generally believed that the sulfoxides can be oxidized to sulfones by high-valent iron-oxo species (Eqs. (10) and (11)) [49,50], which are different from the $SO_4^{\cdot -}$-induced and $HO^{\cdot}$-induced products [28]. If there was sulfones generation in the titanomagnetite/PDS system, it could provide convictive evidence for the formation of high-valent iron-oxo species. In this study, we used aromatic sulfoxide (PMSO) as probe compound. Methyl phenyl sulfone ($PMSO_2$) could be easily analyzed via UPLC/ESI–MS/MS. The analysis method was based on the approach already reported [28]. The details are supplied in the SI Text S4. In this work, 100 μM PMSO were added in titanomagnetite/PDS system. The initial pH of 100 μM PMSO solution was 6.4. After known amounts of titanomagnetite and PDS added, the pH quickly changed to 3.0. In other words, although the initial pH was 6.4, the pH in the whole process was around 3.0. The reaction condition was similar to ATZ removal (i.e., initial pH = 6.3, pH in reaction process was 3.0). The high-valent iron-oxo species are strong oxidants in both acidic and alkaline conditions. In literature, the density functional theory calculation results about the reactivity of high-valent iron-oxo species with organics showed that the oxidation ability of high-valent iron-oxo species is much stronger in acidic conditions than that in alkaline conditions [51,52]. Thus, under that pH condition, high-valent iron-oxo species have strong oxidizing properties.

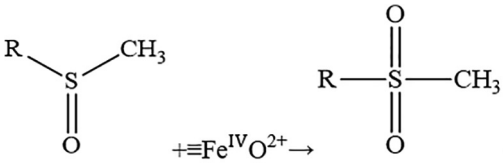

(10)

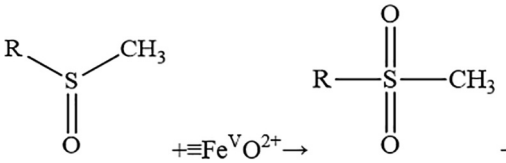

(11)

Fig. 5a shows the extracted ion current (XIC), MS/MS spectrum of $PMSO_2$ standard and total ion chromatogram (TIC) in the negative ESI mode. As expected, $PMSO_2$ was detected when PMSO was treated in the titanomagnetite/PDS system (Fig. 5(b)). To confirm that the generation of $PMSO_2$ was not attributed to the contribution of $SO_4^{\cdot -}$ and $HO^{\cdot}$, control experiment was conducted in the Fe_3O_4/PDS system. From Fig. S7, no spectra were displayed at the retention time of 2.05 min in Fe_3O_4/PDS system, indicating $PMSO_2$ in titanomagnetite/PDS system was formed not because of the $SO_4^{\cdot -}$ and $HO^{\cdot}$. Thus, high-valent iron-oxo species must be formed in titanomagnetite/PDS system. Furthermore, dissolved irons were not detected by the analysis of ICP-MS, indicating surface reaction for the generation of high-valent iron-oxo species. The surface reaction of the generation of high-valent iron-oxo species might be attributed to the natural crystal structure of the titanomagnetite.

3.5. Reaction mechanism of titanomagnetite/PDS system

Based on the above results, both free radicals and non-radicals were generated in titanomagnetite/PDS system. In general, the non-radical generation process always undergoes a two-electron transfer pathway [53]. Besides, both surface ≡Fe(II) and ≡Fe(III) were involved in this

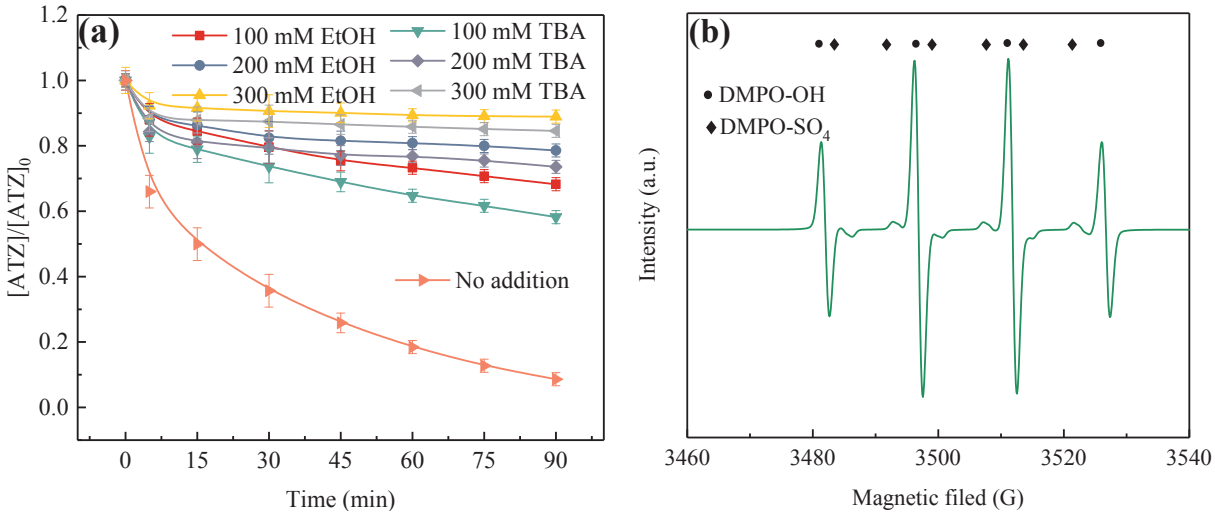

Fig. 4. Effect of TBA and EtOH (a) on the ATZ removal and EPR spectra (b) in the titanomagnetite/PDS system. ($[ATZ]_0$ = 10 mg/L, $[PDS]_0$ = 5.0 mM, titanomagnetite = 8 g/L, initial pH = 6.3 and stirring rate = 300 rpm).

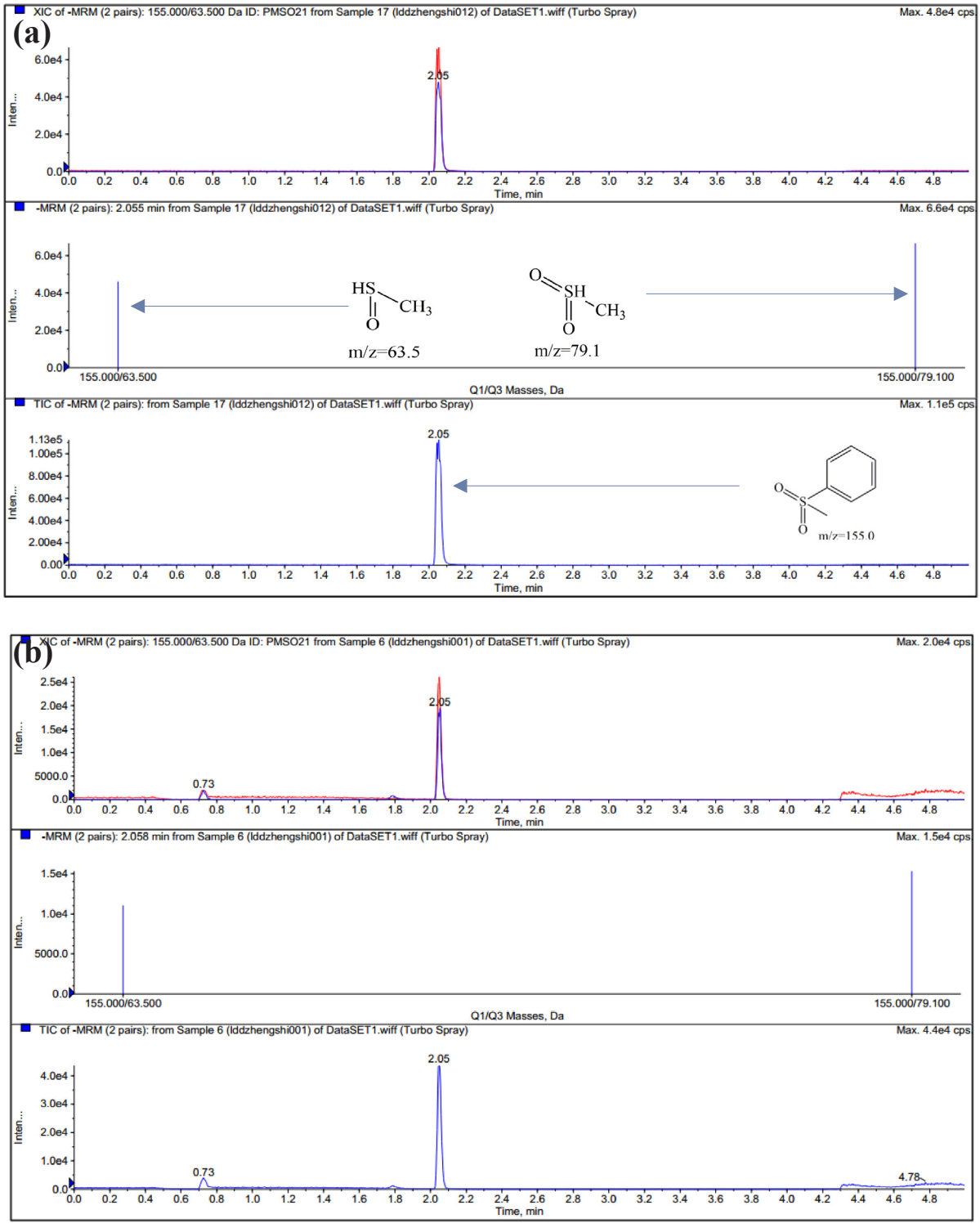

Fig. 5. UPLC/ESI − MS/MS XIC chromatogram, MS/MS spectra and TIC chromatogram of $PMSO_2$ (m/z 155.0) standard in negative ESI mode (a) and UPLC/ESI–MS/MS XIC chromatogram, MS/MS spectra and TIC chromatograms of PMSO treated in the titanomagnetite/PS system (b). ($[PDS]_0$ = 5.0 mM, titanomagnetite = 8 g/L and stirring rate = 300 rpm).

work. Thus, both $\equiv Fe^{IV}=O$ and $\equiv Fe^{V}=O$ might be generated in titanomagnetite/PDS system. In other words, diverse ROS including $SO_4^{\cdot -}$, $HO^{\cdot}$, $\equiv Fe^{IV}=O$ and $\equiv Fe^{V}=O$ were generated simultaneously in titanomagnetite/PDS system. We thought that $SO_4^{\cdot -}$, $HO^{\cdot}$ and $\equiv Fe^{IV}=O$ came from the reaction of surface ≡Fe(II) and PDS, while $\equiv Fe^{V}=O$ came from the reaction of surface ≡Fe(III) and PDS. To confirm the hypotheses of the formation mechanism of ROS, we used 1,10-phenanthroline and sodium citrate as chelating agents to detect the important roles of surface ≡Fe(II) and ≡Fe(III) in the titanomagnetite.

Some literature have reported that ligands exchange could happen between ligand and specific sites of Fe (i.e., ≡Fe-OH) [30,54,55], which then could suppress the capability of catalysts for PDS activation. In other words, the 1,10-phenanthroline could coordinate with Fe(II)

[56], leading to the inactivation on the surface of ≡Fe(II) in the titanomagnetite. In this way, surface ≡Fe(II) could not react with PDS, suppressing the generation of $SO_4^{\cdot -}$, $HO^{\cdot}$ and $\equiv Fe^{IV}=O$. Meanwhile, the sodium citrate could coordinate with Fe(III) [54], forming the metal-carboxyl complex and causing the inactivation on the surface of ≡Fe(III) in the titanomagnetite. Then, the generation of $\equiv Fe^{V}=O$ could be inhibited in the titanomagnetite/PDS system. From Fig. S8, it is clear that ATZ removal efficiency decreased to 17% and 30% with the addition of 1,10-phenanthroline and sodium citrate. respectively. The results manifested that chelating agents indeed suppressed the capability of surface Fe(II) and Fe(III), leading to a decrease of ROS. In other words, both surface ≡Fe(II) and ≡Fe(III) of the titanomagnetite were involved in the formation of ROS. To further investigate whether chelating agents competed for ROS, the concentration changes of 1,10-phenanthroline and sodium citrate were detected by HPLC during the reaction processes. The detection methods were depicted in SI Text S5. Fig. S9 shows that the concentration of 1,10-phenanthroline decreased by less than 1% in the whole process. The decreased concentration of 1,10-phenanthroline manifested the successful ligands exchange between 1,10-phenanthroline and surface of ≡Fe(II) in the titanomagnetite. Due to the constant concentration of 1,10-phenanthroline measured, 1,10-phenanthroline did not react with ROS. Besides, Fig. S10 shows that the peak intensity of $PMSO_2$ in the titanomagnetite/PDS system obviously decreased with the addition of 1,10-phenanthroline (Fig. S10(a)). Furthermore, the spectra of DMPO-OH and DMPO-SO_4 in the titanomagnetite/PDS system were not observed with the addition of 1,10-phenanthroline (Fig. S10(b)). Thus, the decreased ATZ removal efficiency could be attributed to the decrease of ROS rather than competing for ROS after 1,10-phenanthroline addition.

However, the situation changed when sodium citrate added in titanomagnetite/PDS system. Fig. S9 depicts that the concentration of sodium citrate declined slightly when the titanomagnetite/PDS system added sodium citrate. To better explain the decreased concentration of sodium citrate, high-valent iron-oxo species and free radicals were detected in titanomagnetite/PDS systems after adding sodium citrate. From Fig. S11 (a), the peak intensity of $PMSO_2$ with the addition of sodium citrate decreased. Besides, EPR experiments (Fig. S11(b)) show that $SO_4^{\cdot -}$ and $HO^{\cdot}$ still generated in titanomagnetite/PDS systems after adding sodium citrate. In previous work, it was reported that sodium citrate can react with $HO^{\cdot}$ with high reaction rate ($k_{(\text{sodium citrate}/HO)^{\cdot}} = 3.2 \times 10^8 (L \cdot mol^{-1} s^{-1})$) [54], but it does not react with high-valent iron-oxo species [30]. In other words, the decreased concentration of sodium citrate could be explained as the high reaction rate between $HO^{\cdot}$ and sodium citrate, rather than between sodium citrate and high-valent iron-oxo species. Thus, the decreased concentration of $PMSO_2$ (Fig. S11(a)) could be certainly attributed to the absence of $\equiv Fe^{V}=O$ after adding sodium.

In short terms, only $\equiv Fe^{V}=O$ was generated after adding 1,10-phenanthroline addition, while $SO_4^{\cdot -}$, $HO^{\cdot}$ and $\equiv Fe^{IV}=O$ still existed after adding sodium citrate. All of the above results were consistent with our hypothesis. In addition, since Fe did not dissolve in the effluent, homogeneous catalysis was not involved in this study. The reaction mechanism of titanomagnetite/PDS system could be proposed as two parts (Fig. 6):

(i) the surface ≡Fe(II) reacted with PDS to generate free radicals: The formation of free radicals undergoes a single-electron transfer process. The decreased ATZ removal efficiency in the titanomagnetite/PDS system after adding chelating agents suggested that surface ≡Fe(II) was the main catalytic component to activate PDS generating $SO_4^{\cdot -}$ and $HO^{\cdot}$ (Eqs. (6), (7) and (12)). The surface ≡Fe(II) of titanomagnetite would not participate in the reaction after it complexed with 1,10-phenanthroline. Thus, the production of $SO_4^{\cdot -}$ and $HO^{\cdot}$ would be suppressed, leading to a decrease of ATZ removal efficiency. However, ≡Fe (III) could hardly react with PDS to produce free radicals. Thus, the activity of surface ≡Fe (III) for free radicals' generation could be ignored.

(ii) the surface ≡Fe(II) and ≡Fe (III) reacted with PDS to generate high-valent iron-oxo species: The formation of high-valent iron-oxo species undergoes a two-electron transfer course. $PMSO_2$ was formed when PMSO was added into the titanomagnetite/PDS system suggesting that high-valent iron-oxo species existed in the reaction process. Furthermore, the formation of $PMSO_2$ could be detected when 1,10-phenanthroline and citrate were added. Thus, both $\equiv Fe^{IV}=O$ and $\equiv Fe^{V}=O$ were generated in titanomagnetite/PDS system. The generation of high-valent iron-oxo species indicated that the surface ≡Fe (II) and ≡Fe (III) have oxygen acceptor sites. Thus, the formation of high-valent iron-oxo species could be illustrated as: the surface ≡Fe(II) was oxidized by PDS to produce $\equiv Fe^{IV}=O$, while surface ≡Fe (III) reacted with PDS to produce $\equiv Fe^{V}=O$. Additionally, ≡Fe(III) would be formed on the surface of titanomagnetite when surface of ≡Fe(II) reacted with PDS. Those ≡Fe(III) could then be used in the formation of $\equiv Fe^{V}=O$. Finally, the generated $SO_4^{\cdot -}$, $HO^{\cdot}$, $\equiv Fe^{IV}=O$ and $\equiv Fe^{V}=O$ reacted with ATZ in a synergistic manner.

$$\equiv Fe(II) + S_2O_8^{2-} \rightarrow \equiv Fe(III) + SO_4^{\cdot -} + SO_4^{2-} \quad (12)$$

3.6. Recyclability of titanomagnetite

To examine the recyclability of the titanomagnetite, life tests were performed for five cycles. The titanomagnetite was recycled in two different ways: (1) titanomagnetite was directly separated by magnetic separation after each run; (2) titanomagnetite was firstly magnetically separated, and then ultrasonically cleaned to remove adsorbate from titanomagnetite surface. Interestingly, the ATZ removal efficiency varied with the recycling method. Fig. 7(a) shows that the ATZ removal efficiency was 92%, 74%, 68%, 65%, and 57%, respectively, if titanomagnetite was directly magnetically separated after each run. However, if 30 min of ultrasound treatment (power: 70 W, frequency: 19.87 kHz) was used after each run, ATZ removal efficiency (Fig. 7(b)) was 92%, 89%, 89%, 86% and 85%, respectively. This could be concluded that the recycle method influenced titanomagnetite recyclability.

Previous study showed that SO_4^{2-} in the UV-LED/ilmenite/PDS system had been deposited on ilmenite surface after multiple-use, which deactivated the catalytic capacity of ilmenite [57]. Therefore, the similar passivation layer might be generated on the surface of titanomagnetite, if titanomagnetite was directly magnetically separated after each run. To confirm the assumption, XPS and XRD analysis was carried out. Fig. 7(c) compares the XPS fitting results of S 2p core level of the raw titanomagnetite, directly collected titanomagnetite and

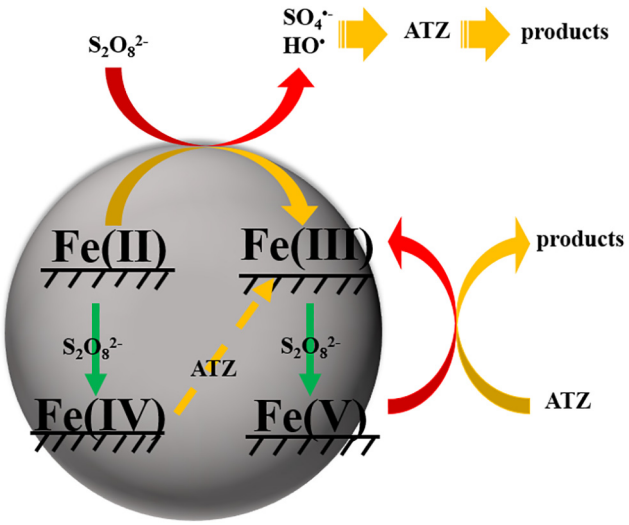

Fig. 6. Reaction mechanism for the ATZ removal by titanomagnetite/PDS system.

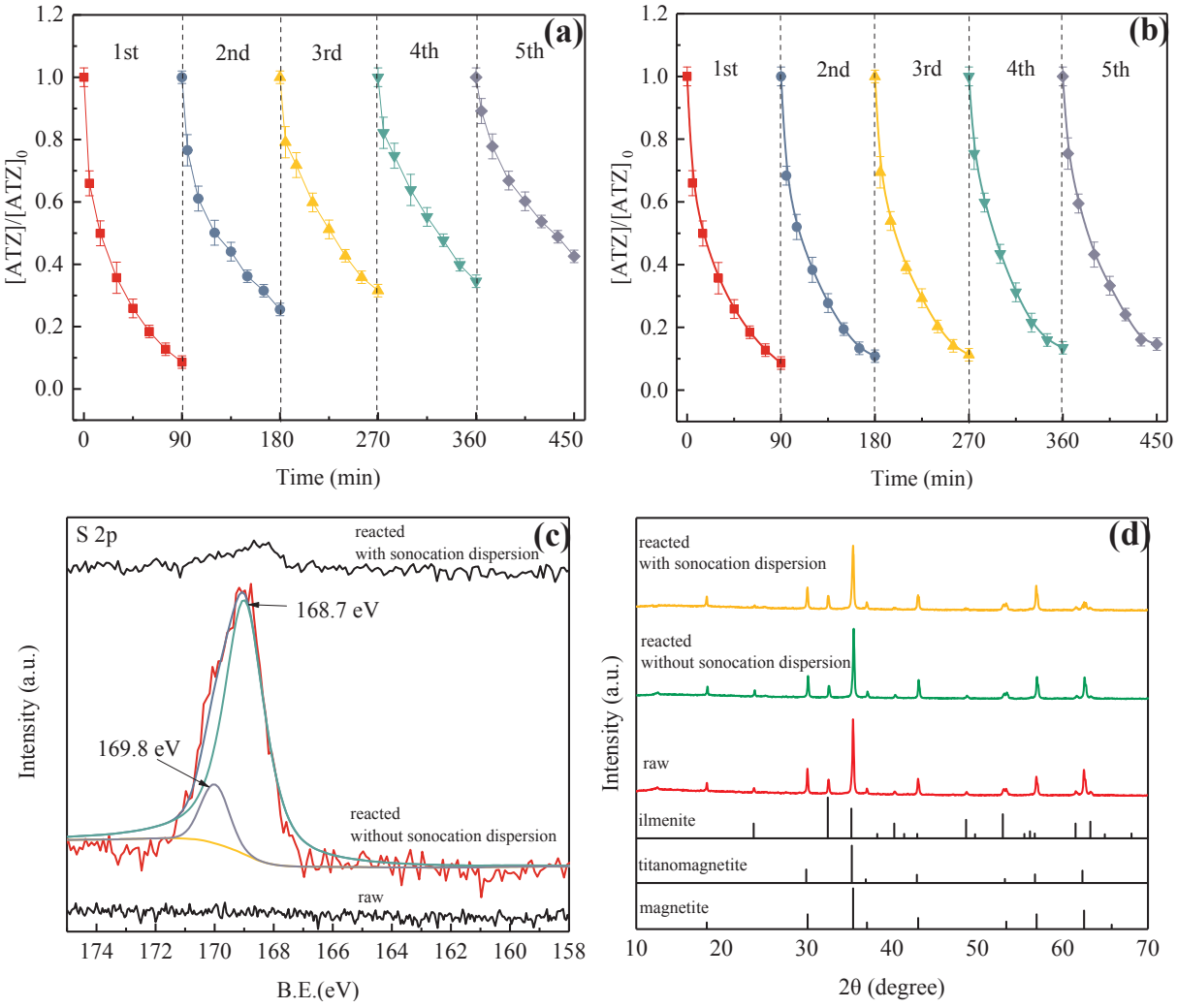

Fig. 7. Recyclability of titanomagnetite: titanomagnetite was directly magnetically separated after each run (a); titanomagnetite was magnetically separated and then used ultrasound treatment (b); XPS spectra of S (c); XRD spectra (d) of the raw titanomagnetite and two kinds of reacted titanomagnetite after five-cycles use ($[ATZ]_0$ = 10 mg/L, $[PDS]_0$ = 5.0 mM, titanomagnetite = 8 g/L, initial pH = 6.3 and stirring rate = 300 rpm).

ultrasonically cleaned titanomagnetite. As shown, there were no obvious spectra in the raw titanomagnetite, suggesting the raw titanomagnetite did not contain S. Compared with raw titanomagnetite, peaks of S $2p_{3/2}$ and S $2p_{1/2}$ located at 168.7 eV and 169.8 eV appeared in the directly collected titanomagnetite. We believe that the S originated from PDS ($Na_2S_2O_8$). In addition, an apparent spectrum of S 2p core level was not found in the ultrasonically cleaned titanomagnetite, indicating ultrasonic treatment could effectively remove the absorbed sulphate to recover the activity of the titanomagnetite. Other XPS fitting results, such as Fe 2p, Ti 2p and O 1s, were depicted in Fig. S12. From Fig. S12(a), it is clear that Fe 2p, Ti 2p and O 1s were all contained in these three titanomagnetites regardless of the recycling method. Fig. S12(b) shows the Fe 2p core level of these three samples. There were two peaks located at around 711.0 eV and 712.5 eV, representing the ≡Fe(II) and ≡Fe(III) on the surface sites of titanomagnetite, respectively. For the raw titanomagnetite, the deconvoluted peaks of ≡Fe(II): ≡Fe(III) ratio was 3:2. However, the deconvoluted peaks of ≡Fe(II): ≡Fe(III) ratio changed into 1:1 and 1:2 indirectly collected titanomagnetite and ultrasonically cleaned titanomagnetite. The results proved that titanomagnetite reacted with PDS could change the ratio of ≡Fe(II) and ≡Fe(III). Besides, ≡Fe(II) in the titanomagnetite could be further oxidized to ≡Fe(III) with the ultrasonic treatment.

The Ti 2p core level of these three samples is presented in Fig. S12(c). The results manifested that the peaks of Ti 2p3/2 located around 458.5 eV and Ti 2p1/2 located around 464.3 eV was ≡Ti(IV). Furthermore, the XPS spectra of O 1 s of these three samples are depicted in Fig. S12(d). The peaks around 530.1 eV, 532.0 eV and 533.4 eV were assigned to the lattice oxygen (O_2^-), hydroxyl group (–OH) and the adsorbed H_2O on the surface of titanomagnetite, respectively [58–60]. An obvious change of oxygen species happened when the reused-titanomagnetite recycled with the sonication dispersion after five cycles. Specifically, the content of –OH decreased in ultrasonically cleaned titanomagnetite, suggesting the adsorbed –OH on the surface of titanomagnetite was involved in the reaction process.

Fig. 7(d) shows XRD spectra of the raw titanomagnetite and two kinds of reacted titanomagnetite after five cycles. Obviously, no matter whether the samples were ultrasonically cleaned or not, the main crystalline phases of the reacted samples had not changed, suggesting that crystal structures of titanomagnetite were not changed by ultrasonic treatment. Therefore, the decreased ATZ removal efficiency did not ascribe to the changes of crystal structure of titanomagnetite. Moreover, the target pollutant adsorbed on the used catalyst might also inhibit the catalysts' activity [61]. To examine if ATZ adsorbed on the used titanomagnetite, the used titanomagnetite was soaked in the deionized water and treated with ultrasound (power: 70 W, frequency: 19.87 kHz). After 30 min of ultrasonication, the effluent was detected by HPLC. The testing results suggested that ATZ was indeed adsorbed

on the titanomagnetite, which provided an indirect proof for the decreased catalytic activity by adsorbed ATZ. However, ultrasonic treatment could effectively remove the adsorbate to maintain the activity of titanomagnetite.

To figure out how the passivation layer inhibited the production of ROS, experiments of quenching and measure of high-valent iron-oxo species were conducted. Fig. S13 shows that ATZ removal efficiency was decreased from 74% to 18% and 25% with the addition of 100 mM of EtOH and TBA, suggesting that $SO_4^{\cdot -}$ and $HO^{\cdot}$ still formed in the reused-titanomagnetite/PDS system even though the passivation layer existed on the catalyst. The UPLC/ESI–MS/MS result of the measure of $PMSO_2$ (Fig. S14) suggested that only very few high-valent iron-oxo species were formed in the reused-titanomagnetite/PDS system. In other words, the passivation layer mainly hindered the generation of high-valent iron-oxo species.

3.7. Possible degradation pathway of ATZ

As shown in Table S3, ten intermediates of ATZ were detected by UPLC-QTOF-MS/MS. Additionally, bond length and bond energy of ATZ was calculated by density functional theory (DFT, Gaussian 09). The method used in this study came from Cheng's group [62]. The calculated results were listed in Table S4. The results suggested that the bonds of C(6)-Cl(14), C(8)-N(7), C(11)-N(10) and C(11)-C(12) were more susceptible to cleavage than other bonds (Fig. S15). Besides, the TIC chromatogram and mass spectra of detected intermediates are presented in Fig. S17–S27. According to these intermediates detected in this study, five degradation pathways ((1) side-chain dealkylation; (2) dechlorination–hydroxylation; (3) side-chain alkylic-oxidation; (4) side-chain alkylic-hydroxylation and (5) side-chain olefination) were proposed for ATZ degradation.

For the Scheme I (Fig. 8), CAIT (*m/z* 188), CEAT (*m/z* 174) and CAAT (*m/z* 146) were generated due to the attack of ROS on the side ethylamino or *iso*-propylamino chains of ATZ [63]. Combined with the bond length and energy of C(8)-N(7) and C(11)-N(10) (Table S4), it was clear that these two bonds were easily cleaved, leading to the generation of dealkylation products. Besides, CAIT (*m/z* 188) and CEAT (*m/z* 174) could respectively take off the *iso*-propylamino and ethylamino to generate CAAT (*m/z* 146). For Scheme II, dechlorination-hydroxylation reaction occurred on ATZ to produce OEIT (*m/z* 198) by the attack of ROS. According to the results of bond length, the bond length of C(6)-Cl (14) was the largest in ATZ (1.763 Å), suggesting the bond of C(6)-Cl (14) was susceptible to cleavage. As oxidation reaction proceeded, olefination occurred to form OVIT (*m/z* 196). In addition, AITO (*m/z* 170) was formed by dealkylation. For Scheme III, CNIT (*m/z* 232) was a derivative of alkylic-hydroxylation, in which an alkyl group is hydroxylated by substitution of a hydrogen atom with a hydroxyl group. Besides, CNIT (*m/z* 232) could further form an aldehyde product (CDIT (*m/z* 230)) by oxidation of the ROS. Then, dechlorination-hydroxylation reaction could further happen to form ODIT (*m/z* 212). Furthermore, according to the bond length (1.436 Å) and energy (3.900 eV) of N(10)-C(11), N(10)-C(11) was easier cleaved to generate AITO (*m/z* 170). OAAT (*m/z* 128) could be generated from CAAT (*m/z* 146) and AITO (*m/z* 170). There were two generation pathways of OAAT (*m/z* 128). CAAT (*m/z* 146) formed OAAT (*m/z* 128) via the effect of dechlorination–hydroxylation, while AITO (*m/z* 170) produced OAAT (*m/z* 128) via deprivation of *iso*-propylamino. The detection intermediates were well matched with results of Gaussian 09, and well-illustrated that ROS in the titanomagnetite/PDS system promoted the decomposition of ATZ. Additionally, the NO_3^- in the effluent detected by ion chromatography system was 3.35 mg/L, also indicating the oxidation of ATZ in the titanomagnetite/PDS system.

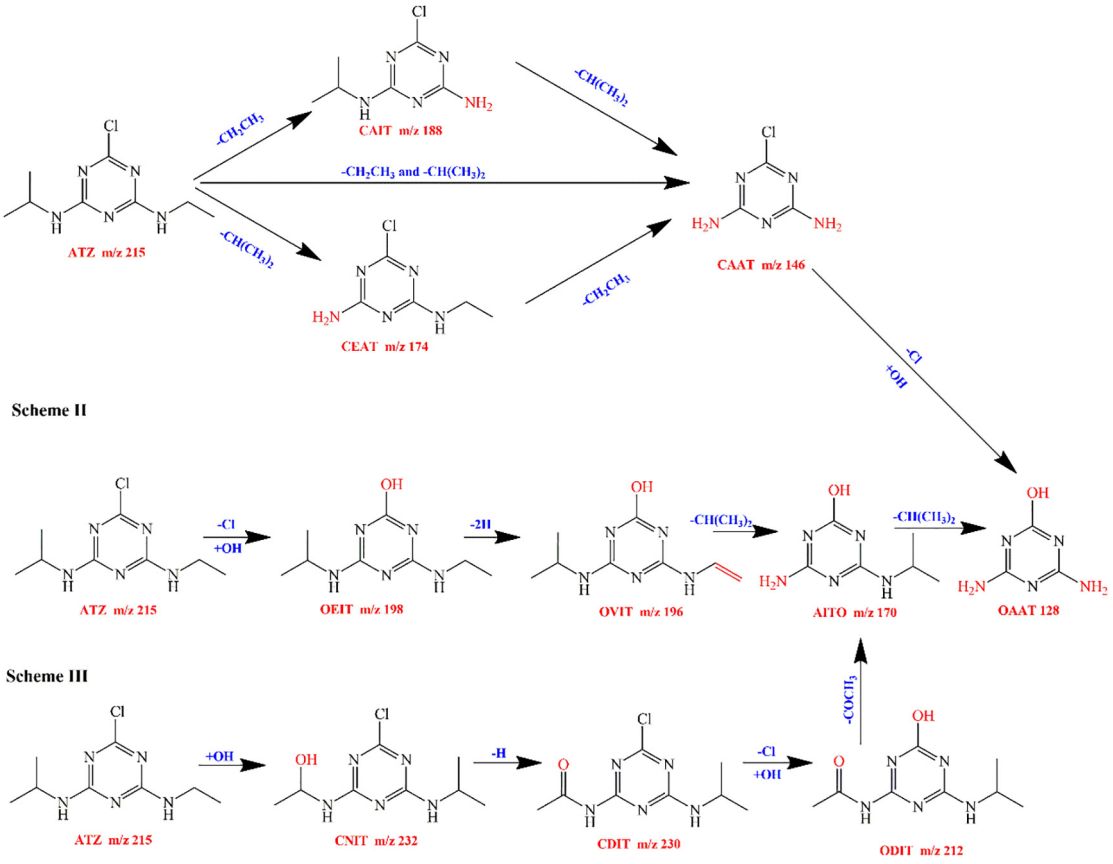

Fig. 8. Degradation pathway of ATZ in the titanomagnetite/PDS system.

4. Conclusions

In summary, this work introduced a natural iron-based mineral, titanomagnetite, as a PDS activator to remove ATZ. ATZ removal efficiency showed a strong dependence on the titanomagnetite concentration (0–10 g/L), PDS concentration (0–10 mM) and initial pH (3.0–11.0) at experimental conditions. The results of quenching experiments, EPR spectra and UPLC/ESI − MS/MS spectra showed its efficient activity visibly enhanced the ATZ removal due to the production of ROS. The mechanism of the titanomagnetite/PDS system included the single-electron transfer and two-electron transfer reactions. Proved by experiments, ROS in the titanomagnetite/PDS systems generated from surface reaction, containing $SO_4^{\cdot -}$, $HO^{\cdot}$, $\equiv Fe^{IV}=O$ and $\equiv Fe^{V}=O$. The generation of $SO_4^{\cdot -}$ and $HO^{\cdot}$ followed a single-electron transfer process, while the formation of $\equiv Fe^{IV}=O$ and $\equiv Fe^{V}=O$ underwent a two-electron transfer course. The surface ≡Fe(II) reacting with PDS not only generated $SO_4^{\cdot -}$ and $HO^{\cdot}$, but also produced $\equiv Fe^{IV}=O$. As for $\equiv Fe^{V}=O$, it was an oxidative product of surface ≡Fe (III). In general, the reaction of the surface ≡Fe (II) and ≡Fe (III) reacted with PDS affected the removal efficiency of ATZ in a synergistic manner. Besides, the passivation layer was generated during the PDS-activated process, which could inhibit the generation of ROS, causing a decrease of the ATZ removal efficiency. However, the passivation layer could be removed through sonication dispersion method. In addition, five degradation pathways of ATZ were proposed via UPLC-QTOF-MS/MS and Gaussian 09 analyses. In general, this work investigated the generation of ROS in depth, which would urge us to re-evaluate the contribution of high-valent iron-oxo species in the PDS-activated processed when iron-based materials used.

Declaration of Competing Interest

The authors declare that they have no known competing financial interests or personal relationships that could have appeared to influence the work reported in this paper.

Acknowledgments

The authors would like to acknowledge the financial support from National Natural Science Foundation of China (No. 51878423), National Natural Science Foundation of China (No. 21808146), Fundamental Research Funds for the Central Universities (No. 2018SCUH0071) and Excellent Youth Foundation of Sichuan Scientific Committee (No. 2019JDJQ0005).

Appendix A. Supplementary data

Supplementary data to this article can be found online at https://doi.org/10.1016/j.cej.2020.124165.

References

[1] H. Zhang, X. Liu, J. Ma, C. Lin, C. Qi, X. Li, Z. Zhou, G. Fan, Activation of peroxymonosulfate using drinking water treatment residuals for the degradation of atrazine, J. Hazard Mater. 344 (2018) 1220–1228.
[2] K.B. Delwiche, J. Lehmann, M.T. Walter, Atrazine leaching from biochar-amended soils, Chemosphere 95 (2014) 346–352.
[3] C. Wang, Z. Guo, R. Hong, J. Gao, Y. Guo, C. Gu, A novel method for synthesis of polyaniline and its application for catalytic degradation of atrazine in a Fenton-like system, Chemosphere 197 (2018) 576–584.
[4] A.M. Schmidt, N. Sengupta, C.A. Saski, R.E. Noorai, W.S. Baldwin, RNA sequencing indicates that atrazine induces multiple detoxification genes in Daphnia magna and this is a potential source of its mixture interactions with other chemicals, Chemosphere 189 (2017) 699–708.
[5] F. Yang, W. Zhang, J. Li, S. Wang, Y. Tao, Y. Wang, Y. Zhang, The enhancement of atrazine sorption and microbial transformation in biochars amended black soils, Chemosphere 189 (2017) 507–516.
[6] Y. Ji, C. Dong, D. Kong, J. Lu, New insights into atrazine degradation by cobalt catalyzed peroxymonosulfate oxidation: kinetics, reaction products and transformation mechanisms, J. Hazard. Mater. 285 (2015) 491–500.
[7] Y. Ji, C. Dong, D. Kong, J. Lu, Q. Zhou, Heat-activated persulfate oxidation of atrazine: Implications for remediation of groundwater contaminated by herbicides, Chem. Eng. J. 263 (2015) 45–54.
[8] D. Zadaka, S. Nir, A. Radian, Y.G. Mishael, Atrazine removal from water by polycation-clay composites: effect of dissolved organic matter and comparison to activated carbon, Water Res. 43 (2009) 677–683.
[9] J.B. Sass, A. Colangelo, European Union bans atrazine, while the United States negotiates continued use, Int. J. Occup. Environ. Health 12 (2006) 260–267.
[10] H.V. Lutze, J. Brekenfeld, S. Naumov, C. von Sonntag, T.C. Schmidt, Degradation of perfluorinated compounds by sulfate radicals – new mechanistic aspects and economical considerations, Water Res. 129 (2018) 509–519.
[11] Q. Zhao, Q. Mao, Y. Zhou, J. Wei, X. Liu, J. Yang, L. Luo, J. Zhang, H. Chen, H. Chen, L. Tang, Metal-free carbon materials-catalyzed sulfate radical-based advanced oxidation processes: a review on heterogeneous catalysts and applications, Chemosphere 189 (2017) 224–238.
[12] S.P. Mezyk, K.A. Rickman, G. Mckay, C.M. Hirsch, X. He, D.D. Dionysiou, Remediation of Chemically-Contaminated Waters Using Sulfate Radical Reactions: Kinetic Studies, 2011.
[13] T. An, H. Yang, G. Li, W. Song, W.J. Cooper, X. Nie, Kinetics and mechanism of advanced oxidation processes (AOPs) in degradation of ciprofloxacin in water, Appl. Catal. B 94 (2010) 288–294.
[14] K.A. Rickman, S.P. Mezyk, Kinetics and mechanisms of sulfate radical oxidation of beta-lactam antibiotics in water, Chemosphere 81 (2010) 359–365.
[15] G.P. Anipsitakis, D.D. Dionysiou, Transition metal/UV-based advanced oxidation technologies for water decontamination, Appl. Catal. B 54 (2004) 155–163.
[16] Q. Liu, Z. Zheng, X. Yang, X. Luo, J. Zhang, B. Zheng, Effect of factors on decolorization of azo dye methyl orange by oxone/natural sunlight in aqueous solution, Environ. Sci. Pollut. Res. 19 (2012) 577–584.
[17] X. Chen, J. Chen, X. Qiao, D. Wang, X. Cai, Performance of nano-Co3O4/peroxymonosulfate system: kinetics and mechanism study using Acid Orange 7 as a model compound, Appl. Catal. B 80 (2008) 116–121.
[18] F. Ghanbari, M. Moradi, Application of peroxymonosulfate and its activation methods for degradation of environmental organic pollutants: Review, Chem. Eng. J. 310 (2017) 41–62.
[19] S. Wacławek, H.V. Lutze, K. Grübel, V.V.T. Padil, M. Černík, D.D. Dionysiou, Chemistry of persulfates in water and wastewater treatment: a review, Chem. Eng. J. 330 (2017) 44–62.
[20] Q. Chen, L. Chen, J. Qi, Y. Tong, Y. Lv, C. Xu, J. Ni, W. Liu, Photocatalytic degradation of amoxicillin by carbon quantum dots modified K2Ti6O13 nanotubes: effect of light wavelength, Chin. Chem. Lett. 30 (2019) 1214–1218.
[21] Y. Ji, D. Kong, J. Lu, H. Jin, F. Kang, X. Yin, Q. Zhou, Cobalt catalyzed peroxymonosulfate oxidation of tetrabromobisphenol A: kinetics, reaction pathways, and formation of brominated by-products, J. Hazard. Mater. 313 (2016) 229–237.
[22] Y. Yao, H. Chen, J. Qin, G. Wu, C. Lian, J. Zhang, S. Wang, Iron encapsulated in boron and nitrogen codoped carbon nanotubes as synergistic catalysts for Fenton-like reaction, Water Res. 101 (2016) 281–291.
[23] H. Zhang, Q. Ji, L. Lai, G. Yao, B. Lai, Degradation of p-nitrophenol (PNP) in aqueous solution by mFe/Cu-air-PS system, Chin. Chem. Lett. 30 (2019) 1129–1132.
[24] S. Wacławek, V.V.T. Padil, M. Černík, Major advances and challenges in heterogeneous catalysis for environmental applications: a review, Ecol. Chem. Eng. S 25 (2018) 9–34.
[25] A. Tsitonaki, B. Petri, M. Crimi, H. MosbÆK, R.L. Siegrist, P.L. Bjerg, In Situ chemical oxidation of contaminated soil and groundwater using persulfate: a review, Crit. Rev. Environ. Sci. Technol. 40 (2010) 55–91.
[26] L.W. Matzek, K.E. Carter, Activated persulfate for organic chemical degradation: a review, Chemosphere 151 (2016) 178–188.
[27] J. Li, Y. Li, Z. Xiong, G. Yao, B. Lai, The electrochemical advanced oxidation processes coupling of oxidants for organic pollutants degradation: a mini-review, Chin. Chem. Lett. 30 (2019) 2139–2146.
[28] Z. Wang, J. Jiang, S. Pang, Y. Zhou, C. Guan, Y. Gao, J. Li, Y. Yang, W. Qiu, C. Jiang, Is sulfate radical really generated from peroxydisulfate activated by iron(II) for environmental decontamination? Environ. Sci. Technol. 52 (2018) 11276–11284.
[29] Z. Wang, W. Qiu, S.-Y. Pang, Y. Zhou, Y. Gao, C. Guan, J. Jiang, Further understanding the involvement of Fe(IV) in peroxydisulfate and peroxymonosulfate activation by Fe(II) for oxidative water treatment, Chem. Eng. J. 371 (2019) 842–847.
[30] H. Li, C. Shan, B. Pan, Fe(III)-doped g-C3N4 mediated peroxymonosulfate activation for selective degradation of phenolic compounds via high-valent iron-oxo species, Environ. Sci. Technol. 52 (2018) 2197–2205.
[31] C. Liang, C.F. Huang, N. Mohanty, R.M. Kurakalva, A rapid spectrophotometric determination of persulfate anion in ISCO, Chemosphere 73 (2008) 1540–1543.
[32] Z. Xiong, B. Lai, P. Yang, Insight into a highly efficient electrolysis-ozone process for N, N-dimethylacetamide degradation: quantitative analysis of the role of catalytic ozonation, fenton-like and peroxone reactions, Water Res. 140 (2018) 12–23.
[33] H. Wang, S. Yuan, J. Zhan, Y. Wang, G. Yu, S. Deng, J. Huang, B. Wang, Mechanisms of enhanced total organic carbon elimination from oxalic acid solutions by electro-peroxone process, Water Res. 80 (2015) 20–29.
[34] C. Liu, L. Lai, X. Yang, Sewage sludge conditioning by Fe(II)-activated persulphate oxidation combined with skeleton builders for enhancing dewaterability, Water Environ. J. 30 (2016) 96–101.
[35] Z. Lin, Z. Zhen, L. Ren, J. Yang, C. Luo, L. Zhong, H. Hu, Y. Liang, Y. Li, D. Zhang, Effects of two ecological earthworm species on atrazine degradation performance and bacterial community structure in red soil, Chemosphere 196 (2018) 467–475.
[36] S. Andleeb, Z. Jiang, K.U. Rehman, E.K. Olajide, Z. Ying, Influence of Soil pH and Temperature on Atrazine Bioremediation, J. Northeast Agric. Univ. (English Edition) 23 (2016) 12–19.

[37] S. Wu, H. He, X. Li, C. Yang, G. Zeng, B. Wu, S. He, L. Lu, Insights into atrazine degradation by persulfate activation using composite of nanoscale zero-valent iron and graphene: performances and mechanisms, Chem. Eng. J. 341 (2018) 126–136.
[38] H.V. Lutze, S. Bircher, I. Rapp, N. Kerlin, R. Bakkour, M. Geisler, C. von Sonntag, T.C. Schmidt, Degradation of chlorotriazine pesticides by sulfate radicals and the influence of organic matter, Environ. Sci. Technol. 49 (2015) 1673–1680.
[39] J.L. Acero, K. Stemmler, U.V. Gunten, Degradation kinetics of atrazine and its degradation products with ozone and OH radicals: a predictive tool for drinking water treatment, Environ. Sci. Technol. 34 (2000) 591.
[40] R. Loos, G. Locoro, S. Comero, S. Contini, D. Schwesig, F. Werres, P. Balsaa, O. Gans, S. Weiss, L. Blaha, M. Bolchi, B.M. Gawlik, Pan-European survey on the occurrence of selected polar organic persistent pollutants in ground water, Water Res. 44 (2010) 4115–4126.
[41] L. Lai, J. Yan, J. Li, B. Lai, Co/Al 2 O 3 -EPM as peroxymonosulfate activator for sulfamethoxazole removal: performance, biotoxicity, degradation pathways and mechanism, Chem. Eng. J. 343 (2018) 676–688.
[42] J. Li, M. Xu, G. Yao, B. Lai, Enhancement of the degradation of atrazine through CoFe 2 O 4 activated peroxymonosulfate (PMS) process: kinetic, degradation intermediates, and toxicity evaluation, Chem. Eng. J. 348 (2018) 1012–1024.
[43] L. Lai, H. Zhou, B. Lai, Heterogeneous degradation of bisphenol A by peroxymonosulfate activated with vanadium-titanium magnetite: performance, transformation pathways and mechanism, Chem. Eng. J. 349 (2018) 633–645.
[44] Y. Xu, J. Ai, H. Zhang, The mechanism of degradation of bisphenol A using the magnetically separable CuFe 2 O 4/peroxymonosulfate heterogeneous oxidation process, J. Hazard. Mater. 309 (2016) 87–96.
[45] E. Hayon, A. Treinin, J. Wilf, Electronic spectra, photochemistry, and autoxidation mechanism of the sulfite-bisulfite-pyrosulfite systems. SO2-, SO3-, SO4-, and SO5-radicals, J. Am. Chem. Soc. 94 (1972) 47–57.
[46] A. Jawad, J. Lang, Z. Liao, A. Khan, J. Ifthikar, Z. Lv, S. Long, Z. Chen, Z. Chen, Activation of persulfate by CuOx@Co-LDH: A novel heterogeneous system for contaminant degradation with broad pH window and controlled leaching, Chem. Eng. J. 335 (2018) 548–559.
[47] Y. Zhou, J. Jiang, Y. Gao, J. Ma, S.Y. Pang, J. Li, X.T. Lu, L.P. Yuan, Activation of peroxymonosulfate by benzoquinone: a novel nonradical oxidation process, Environ. Sci. Technol. 49 (2015) 12941.
[48] Y. Yang, G. Banerjee, G.W. Brudvig, J.H. Kim, J.J. Pignatello, Oxidation of organic compounds in water by unactivated peroxymonosulfate, Environ. Sci. Technol. 52 (2018) 5911–5919.
[49] S.Y. Pang, J. Jiang, J. Ma, Oxidation of sulfoxides and arsenic(III) in corrosion of nanoscale zero valent iron by oxygen: evidence against ferryl ions (Fe(IV)) as active intermediates in Fenton reaction, Environ. Sci. Technol. 45 (2011) 307.
[50] O. Pestovsky, S. Stoian, E.L. Bominaar, X. Shan, E. Munck, L. Que Jr., A. Bakac, Aqueous FeIV = O: spectroscopic identification and oxo-group exchange, Angew. Chem. Int. Ed. Engl. 44 (2005) 6871–6874.
[51] T.K. Takehiro Ohta, Yoshihito Shiota, Kazunari Yoshizawa, A theoretical study of alcohol oxidation by ferrate, J. Organic Chem. 66 (2001) 4122–4131.
[52] T. Yang, L. Wang, Y. Liu, Z. Huang, H. He, X. Wang, J. Jiang, D. Gao, J. Ma, Comparative study on ferrate oxidation of BPS and BPAF: Kinetics, reaction mechanism, and the improvement on their biodegradability, Water Res. 148 (2019) 115–125.
[53] L. Gábor, K. József, B. Zsuzsa, K. Alíz, K. Ildikó, B. Dávid, T. Marcell, V. Lilla, F. István, One- versus two-electron oxidation with peroxomonosulfate ion: reactions with iron(II), vanadium(IV), halide ions, and photoreaction with cerium(III), Inorg. Chem. 48 (2009) 1763–1773.
[54] X. Xue, K. Hanna, C. Despas, F. Wu, N. Deng, Effect of chelating agent on the oxidation rate of PCP in the magnetite/H2O2 system at neutral pH, J. Mol. Catal. A: Chem. 311 (2009) 29–35.
[55] X. Hou, X. Huang, F. Jia, Z. Ai, J. Zhao, L. Zhang, Hydroxylamine promoted goethite surface fenton degradation of organic pollutants, Environ. Sci. Technol. 51 (2017) 5118–5126.
[56] Z. Ai, Z. Gao, L. Zhang, W. He, J.J. Yin, Core-shell structure dependent reactivity of Fe@Fe(2)O(3) nanowires on aerobic degradation of 4-chlorophenol, Environ. Sci. Technol. 47 (2013) 5344–5352.
[57] J.E. Silveira, W.S. Paz, P. Garcia-Muñoz, J.A. Zazo, J.A. Casas, UV-LED/ilmenite/persulfate for azo dye mineralization: the role of sulfate in the catalyst deactivation, Appl. Catal. B 219 (2017) 314–321.
[58] Y. Xu, J. Ai, H. Zhang, The mechanism of degradation of bisphenol A using the magnetically separable CuFe2O4/peroxymonosulfate heterogeneous oxidation process, J. Hazard. Mater. 309 (2016) 87–96.
[59] Z. Zsoldos, L. Guczi, Structure and catalytic activity of alumina supported platinum-cobalt bimetallic catalysts. Part 3. Effect of treatment on the interface layer, J. Phys. Chem. 96 (1992) 9393–9400.
[60] C. Tan, N. Gao, Y. Deng, J. Deng, S. Zhou, J. Li, X. Xin, Radical induced degradation of acetaminophen with Fe3O4 magnetic nanoparticles as heterogeneous activator of peroxymonosulfate, J. Hazard. Mater. 276 (2014) 452–460.
[61] J. Miao, J. Sunarso, X. Duan, W. Zhou, S. Wang, Z. Shao, Nanostructured Co-Mn containing perovskites for degradation of pollutants: insight into the activity and stability, J. Hazard. Mater. 349 (2018) 177–185.
[62] C. Chen, S. Yang, Y. Guo, C. Sun, C. Gu, B. Xu, Photolytic destruction of endocrine disruptor atrazine in aqueous solution under UV irradiation: products and pathways, J. Hazard. Mater. 172 (2009) 675–684.
[63] J.A. Khan, X. He, N.S. Shah, H.M. Khan, E. Hapeshi, D. Fatta-Kassinos, D.D. Dionysiou, Kinetic and mechanism investigation on the photochemical degradation of atrazine with activated H2O2, S2O82− and HSO5−, Chem. Eng. J. 252 (2014) 393–403.